ACS APPLIED MATERIALS & INTERFACES

www.acsami.org

Research Article

Stirred Not Shaken: Facile Production of High-Quality, High-Concentration Graphene Aqueous Suspensions Assisted by a Protein

Megan K. Puglia, Sohan Aziz, Kevin M. Brady, Mark O'Neill, and Challa V. Kumar*

Cite This: *ACS Appl. Mater. Interfaces* 2020, 12, 3815−3826

Read Online

ACCESS | Metrics & More | Article Recommendations | Supporting Information

ABSTRACT: A simple method to produce record concentrations (up to 10 mg mL^{-1}) of high-quality aqueous graphene suspensions by using an ordinary benchtop magnetic stirrer is reported. The shear rates employed here are almost 10 times less than those in previous reports, and graphene is efficiently separated from unexfoliated graphite during the synthesis. Systematic optimization of synthesis parameters, such as pH, protein concentration, temperature, stirrer speed, and volume of solution, afforded efficient conversion (100%) of graphite to graphene−aqueous suspensions. The synthesis is readily scaled-up with a continuous flow reactor where the graphene is produced and separated 24/7, with little or no human intervention. Raman spectroscopy confirmed little to no sp^3 or oxidative defects, and that the graphene nanosheets consisted of three to five layers. The graphene suspensions were coated on aluminum and tested for thermal conductivity applications. The thermal conductivity of our graphene sample was calculated to be 684 W m^{-1} K^{-1}, a value greater than that of a commercial sample. The activation energy measured for shear exfoliation by stirring was found to be over 45 billion times smaller than the corresponding thermal activation energy, affording physical insight into the process. We hypothesize that stirring selectively populates translational states that are necessary for exfoliation and thus requires far less energy than conventional exfoliation methods, where the energy is uniformly distributed among all available modes. Therefore, an efficient, convenient, and inexpensive method for graphene production in limited-resource settings is reported here.

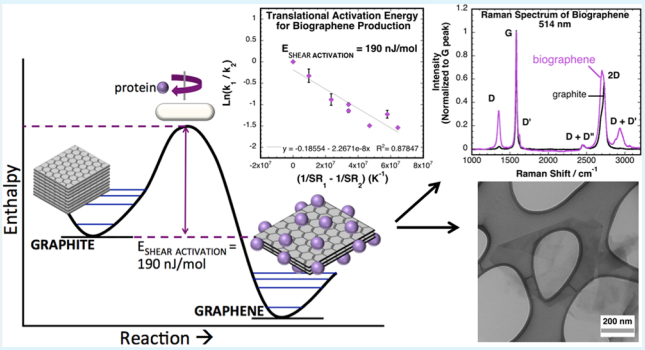

KEYWORDS: *bovine serum albumin, biophilic graphene, mechanism, low-shear synthesis, activation energy*

1. INTRODUCTION

Preparation of high quality graphene suspensions in water, on a large scale, remains a current unmet challenge. In response, we report a simple, inexpensive, and safe top-down synthesis method to produce high-quality graphene (not graphene oxide) suspensions in water, at record concentrations, using a standard benchtop stirrer. The major breakthrough here is the very low shear required to exfoliate graphite to graphene, which is almost 10 times less than those of previous methods. Since its discovery in 2004, graphene's[1] thermal and electrical conductivity properties,[1−5] as well as its optical transparency[6] and tensile strength,[7] have opened the door to seemingly impossible ideas including flexible electronics,[8,9] invisibility cloaks,[10] and space elevators.[11] To date, graphene has been used to create better energy storage devices,[12,13] solar cells,[14] electrodes,[15] photosensitive transistors,[16] and biosensors[17] (to name only a few), dominating the world of materials science. However, these technological advancements have, for the most part, only been actuated on a small scale due to limitations in obtaining large quantities of high-quality graphene.

High-quality single-layer graphene (SLG) is often synthesized using chemical vapor deposition (CVD),[18−23] while few-layer graphene (FLG) has been synthesized with ball milling, sonication, and shear exfoliation.[24−35] Shear exfoliation involves the application of shear forces to delaminate the crystals of graphite into individual graphene sheets or FLG. FLG production by shear exfoliation often requires the use of organic solvents or surfactants.[24−26,34] Surfactants used are toxic or undesirable, and dispersants, such as sodium cholate, gave limited concentrations of expensive FLG.[25−27,35−40] Therefore, producing aqueous suspensions of surfactant-free graphene in large quantities, at low cost, is a major challenge. Surfactant-free graphene suspensions in water were produced earlier by using proteins as dispersants. However, protein-assisted exfoliation

Received: August 24, 2019
Accepted: December 27, 2019
Published: December 27, 2019

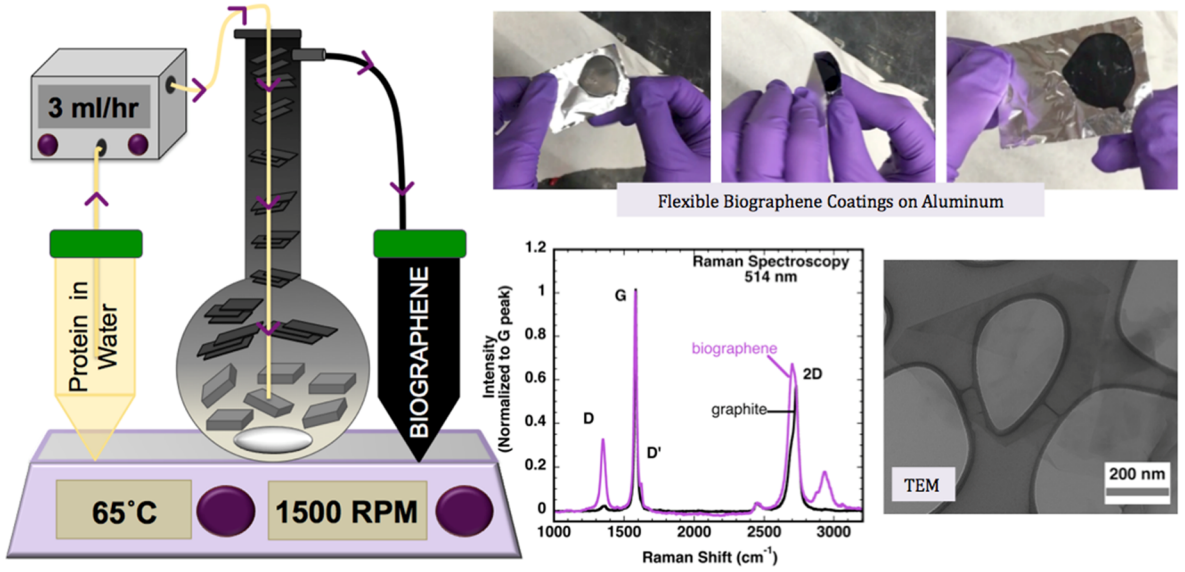

Figure 1. Schematic representation of the biographene continuous flow reactor allowing for continuous collection of few-layer biographene with minimal effort post setup. The quality of the graphene sheets produced this way was confirmed via Raman spectroscopy and transmission electron microscopy. The graphene suspensions were then use to easily fabricate flexible and thermally stable graphene/aluminum coatings.

required high shear forces and resulted in restricted concentrations of FLG suspensions.

The highest yield of FLG–water suspensions obtained with protein-assisted exfoliation was only about 6–7 mg mL^{-1},[37] while the current method produces 10–12 mg mL^{-1} graphene in water with an ordinary benchtop magnetic stirrer. In addition, previous preparations have limited stability, low yield, and require expensive instrumentation and constant attention. The current method uses an ordinary magnetic stirrer to produce aqueous suspensions of FLG without frequent human intervention.

Another major bottleneck of producing aqueous FLG water dispersions has been the scale-up to produce large quantities for biological and other applications. The current approach addresses this issue by using a continuous flow reactor to produce surfactant-free graphene, 24/7, without compromising the high quality, high concentrations, and high conversion of graphite to graphene.

An additional concern in making FLG is the separation of graphene from graphite. Previous methods require tedious, time-consuming centrifugation steps to separate FLG from the unexfoliated graphite. In the current method, FLG is efficiently separated from graphite within the reactor by gravity and requires no further need for centrifugation or purification. This is another novel feature of the current method, which saves time and effort without compromising the quality of graphene while still producing 24/7.

Although many different exfoliation methods of graphite to graphene are known, the energy barriers inherent to these processes have not been delineated before. Hence, we attempt to understand why graphite can be exfoliated under low shear conditions, such as stirring. The simplicity of our synthesis allowed for the calculation of the activation energy for stirring induced exfoliation and for a classical thermal activation energy. In comparing these two values, important physical insights were gained in terms of how directly populating specific graphite translational modes may facilitate efficient graphite exfoliation.

The current method to produce high-quality graphene in water in a flow reactor is shown in Figure 1. The apparatus consists of a peristaltic pump, a round-bottom flask with an elongated neck, and a magnetic stirrer, all connected with basic tubing. The system flows autonomously; therefore, intervention is only needed to add more protein stock solution or solid graphite.

The high quality of the graphene suspensions was confirmed by Raman spectroscopy, indicating few sp^3 defects and no oxidative defects. The morphology, shape, and composition of the sheets were further established by electron microscopy. We have also studied and optimized a number of synthesis conditions in an effort to better understand the exfoliation mechanism and the graphene–protein as well as graphene–water interface. The graphene suspensions were then coated on aluminum to fabricate lightweight heat radiators for applications in space voltaics. Details of our investigations follow.

2. EXPERIMENTAL METHODS

2.1. Continuous Flow Reactor Setup. A 500 mL round-bottom flask connected to a 30 cm-long neck with a 1.5 cm diameter was made by a professional glass blower. A $2' \times {}^{3}/_{4}'$ size egg stir bar was added to the bottom, and a glass piece with an inner entrance tube and outer exit tube was fit to the top of the neck. Biographene samples were analyzed with ultraviolet-visible (UV–vis) spectroscopy, Raman spectroscopy, transmission electron microscopy (TEM), scanning electron microscopy/energy-dispersive spectrometry (SEM/EDS), and zeta potential analysis (Supporting Information).

2.2. Removal of Free Protein. Samples of biographene were first centrifuged at 0.2 *g* for 10 min to remove any graphite or many-layered (>12) graphene nanosheets. The supernatant solution was then centrifuged at 17 *g* for 65 min to remove the free BSA. The resulting clear supernatant, containing free BSA, was then removed from the centrifuge tube. The remaining graphene pellet at the bottom was then resuspended in distilled water by vigorous up and down pipetting. This solution was then centrifuged a second time at 17 *g* for 65 min. Again, the supernatant was removed and the pellet was resuspended in distilled water. The pellet could be resuspended in the original volume or a smaller volume to increase the graphene concentration if desired.

2.3. Optimization of Biographene. Optimization studies were completed over a 24 h stir period for all experiments, with one variable being changed at a time. Cylindrical vials (7.4 mL, 1.5 cm diameter) were used in all cases (VWR International, LLC Radnor, PA:

https://dx.doi.org/10.1021/acsami.9b15121
ACS Appl. Mater. Interfaces 2020, 12, 3815–3826

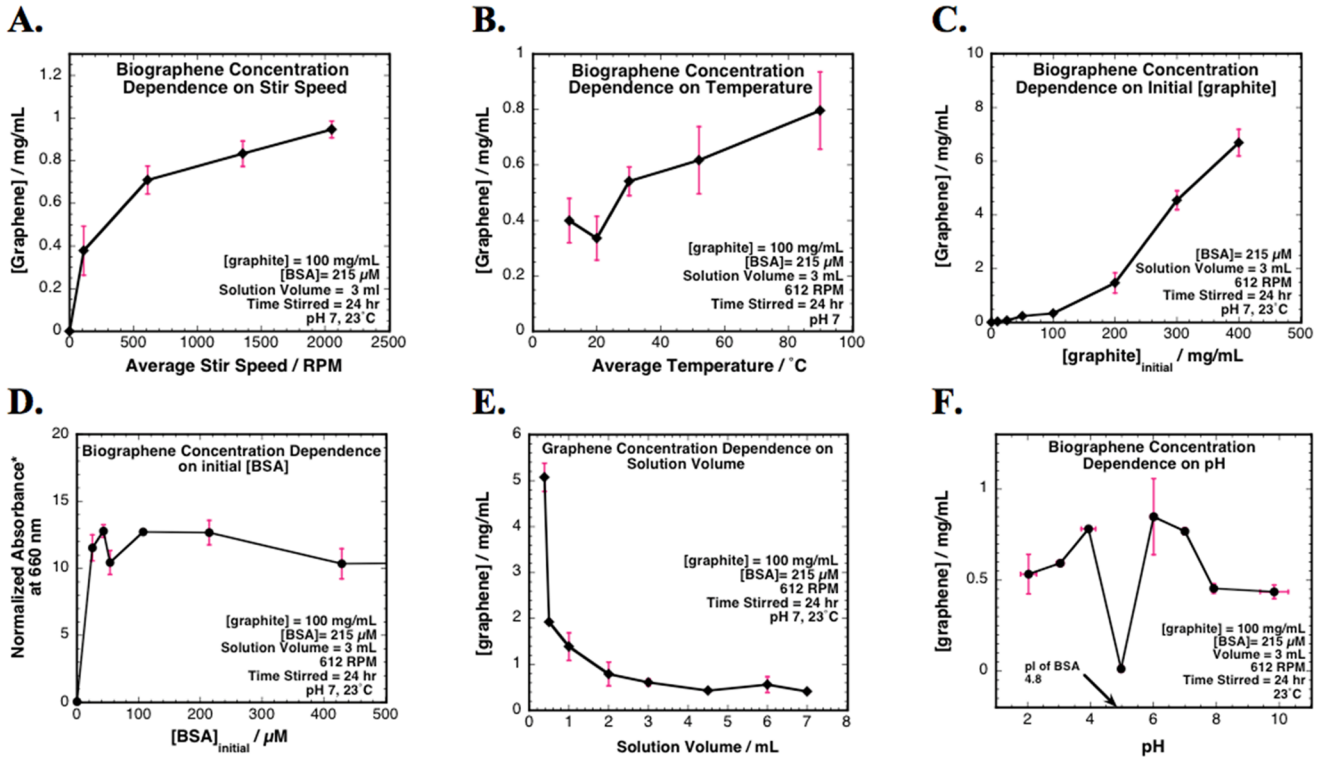

Figure 2. Optimization studies done to determine the amount of biographene produced as (A) stir speed, (B) temperature, (C) initial graphite concentration, (D) initial BSA concentration, (E) solution volume, and (F) pH were varied. All sample absorbances were taken at 660 nm (E = 20.0 mg^{-1} mL cm^{-1}). Unless otherwise indicated, all trials were done with 3 mL of sample volumes, 1.3 cm diameter stir bar, and 7.4 mL vials (vial diameter = 1.5 cm). While varying the initial graphite concentration, the change in volume caused by larger additions of flakes (>300 mg mL^{-1}) was ignored for convenience; therefore, the reported initial concentrations are a slight overestimate. In some cases, error bars are too small to see. *In plot D, the effect of varying [BSA] is plotted as absorbance at 660 nm multiplied by the dilution factor for each solution due to varying extinction coefficients.

VW60910-A) with an octagon cross section stir bar (1/2 inch long by 1/8 inch diameter). Samples were stirred in six vials at a time in the center of an INTLLAB stir plate. In all experiments, the solution volume was given as the volume of BSA solution added to the vial, assuming no added volume from the graphite powder. In the cases where the graphite powder concentration exceeded 300 mg mL^{-1}, the powder caused a slight volume change; thus, the given volume is an underestimate. After samples were stirred for 24 h, they were centrifuged at 0.2 g for 10 min to remove any graphite flakes, and their absorbances at 660 nm were recorded.

2.4. Activation Energy Calculations. Using the concentrations of biographene produced over 24 h of stirring under specific conditions, at different temperatures, an Arrhenius plot was constructed by plotting the natural log of (k_1/k_2) versus $1/T_1 - 1/T_2$ (K^{-1}). Biographene concentration is assumed to be proportional to the rate constant (k). The slope of this plot is equal to $-E_{\text{THERMAL ACTIVATION}}/R$ (R = 8.314 J mol^{-1} K^{-1}). A pseudo-Arrhenius plot was constructed using the shear rate instead of temperature, and the corresponding activation energy for stirring-mediated exfoliation was obtained. The slope obtained for this plot was $-E_{\text{SHEAR ACTIVATION}}/R$ (R = 8.314 J mol^{-1} K^{-1}).

3. RESULTS AND DISCUSSION

3.1. Biographene Synthesis Using a Stir Reactor. The continuous flow reactor (Figure 1) was set up using a 500 mL round-bottom flask with a 30 cm elongated neck to gravity separate the few-layer biographene from the graphite flakes. The flask was loaded with graphite (100 mg mL^{-1}), a stir bar, and the BSA solution (20 mg mL^{-1}, 500 mL). The temperature was set to 65 °C while stirring, and after 1 day, the fresh BSA solution was pumped continuously into the bottom of the reactor while collecting the graphene suspension from the top of the reactor. In this way, 100% of the original graphite flakes put into the reactor are eventually exfoliated into graphene by continual flow of BSA solution through the reactor. A high concentration of 10 mg mL^{-1} graphene was obtained after first centrifuging to remove many-layered nanosheets and then washing off excess protein via centrifugation at 17 g for 65 min (twice) (Figure S1).

Bovine serum albumin (BSA), an inexpensive waste product of the meat industry,[41,42] was chosen here as the surfactant due to previous reported success.[36−38,43−45] BSA has been suggested to aid in stabilizing graphene sheets in water by binding its hydrophobic segments to graphene while exposing its hydrophilic segments to water.[38,44] Previous reports propose that BSA aids in exfoliation due to its ability to bind to graphene via stacking of its aromatic residues onto the sp^2 carbons, as well as a number of the BSA residues adsorbing onto the graphene surface.[43] Additionally, 99 carboxylic acid and 82 amine groups of BSA offer numerous attachment sites for subsequent conjugation chemistry with the protein-loaded graphene.[38,46] In this context, BSA acts as an imperative exfoliating agent and stabilizer; however, all unbound BSA is removed from the graphene to limit deviations from graphene's inherent properties.

To remove free BSA from the solution, samples were centrifuged at 17 g for 65 min, and the supernatant was removed and replaced with distilled water (and the centrifugation process was repeated once more) until there was no detectable protein in the wash (Bradford assay, Figure S2).[47] Unwashed graphene ($[BSA]_i$ = 215 μM) was found to have 5.3 ± 1.4 mg of protein per milligram of graphene, and washed graphene (hereinafter biographene) had 0.9 ± 0.2 mg of protein per milligram of graphene. The protein to graphene

https://dx.doi.org/10.1021/acsami.9b15121
ACS Appl. Mater. Interfaces 2020, 12, 3815−3826

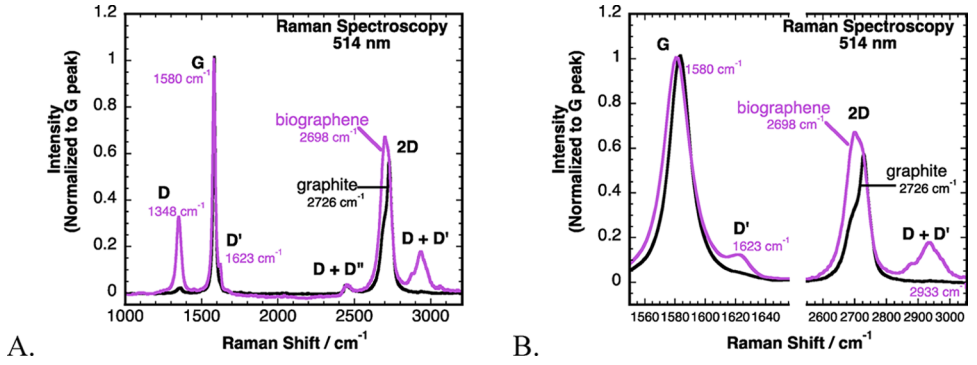

Figure 3. (A) Raman spectra of graphite (black) and biographene (pink). The average of over 100 Raman spectra was used to calculate an average of three to five layers per flake.[25] A 514 nm excitation laser was used for all Raman measurements. (B). Close-up of the D′ and 2D bands from Figure 3A, where biographene's pronounced D′ can be seen and the 2D band shift, from 2726 cm^{-1} in graphite to 2698 cm^{-1} in graphene, is visible.

composition was confirmed via SEM/EDS analysis where the unwashed sample was shown to have a greater nitrogen/carbon ratio (0.2:1) than the biographene sample (0.1:1), indicating the removal of protein from the washed sample (Figure S3 and Table S1). Table S1 also shows the (rough) estimated percent oxygen in our graphene samples to be only about 4−6%, agreeing with our Raman analysis. The amount of remaining BSA after washing was further confirmed using thermogravimetric analysis (TGA) shown in Figure S4. The TGA data shows that the (washed) biographene has 45% protein by weight translating to about 0.8 mg of BSA to 1 mg of graphene.

Ultraviolet−visible absorbance spectroscopy was used to calculate and compare biographene sample concentrations in the flow reactor from day to day using the sample absorbance at 660 nm (Figure S5A). Biographene collected from the flow reactor showed a steady increase in concentration of 0.1 mg mL^{-1} per day at a pump rate of 3 mL h^{-1}. Biographene concentration in the reactor reached a plateau after day 28 with a concentration of 2.5 mg mL^{-1} graphene, and more graphite was added to the reactor when needed (Figure S5B). It is important to note that we monitored our flow reactor for continuous production of biographene for 28 days; however, high concentrations of biographene do not require 28 days processing time and can be made in 24−48 h depending on the parameters used. Biographene concentration was determined using the calculated extinction coefficients at 660 nm (Figure S5C,D). E_{660} values were determined to be 11.9 and 20 mg^{-1} mL cm^{-1} for biographene and unwashed biographene, respectively. It is relevant to note that there is a broad range of extinction coefficients for graphene reported in the literature, which can influence concentration results.

3.2. Optimization of Biographene Synthesis. The influence of different process parameters was investigated by careful testing of biographene production as a function of initial [BSA], initial [graphite], stir speed, reactor temperature, pH, volume of the reaction mixture, and shear rate employed over a stir period of 24 h (Figure 2).

Intuitively, the stir speed has a considerable effect on the graphene production rate (Figure 2A). An increase in rotations per minute allows for an increase in shear rate (eq 1), which facilitates the shearing apart of graphite flakes (Figure S6). In this report, the shear rate was determined by eq 1.[48]

$$\dot{\gamma} = \sqrt{\frac{N_p \rho F^3 d^5}{\eta V}} \quad (1)$$

In eq 1, N_p is the power number,[49] ρ is the density of the solution (kg m^{-3}), F is the rotation frequency of the stir bar (s^{-1}), d is the diameter of the stir bar (m), η is the viscosity of the solution (Pa s), and V is the volume of the solution. This equation most accurately describes the shear rate produced by a two-blade flat paddle impeller, which is used as an approximation for our stir bar system. Further discussion of shear rate calculations can be found in eqs S1−S4 and Table S2.

The temperature of the system is also seen to play a role in graphene production (Figure 2B). Foremost, an increase in temperature can cause a decrease in viscosity of the liquid, as well as an increase in molecular collisions. An added benefit to keeping the graphene reactor at 65 °C is that this temperature will kill most bacteria attempting to grow in the reactor, prolonging your biographene lifetime.[50]

Initial graphite concentration has a profound effect on the graphene production, as was anticipated. Figure 2C shows that an increase in initial graphite concentration resulted in a steep increase in graphene production. Graphite concentrations above 400 mg mL^{-1} were not tested due to the change in solution volume the bulk graphite would cause, as well as the increased resistance caused for the stir bar. The initial graphite concentration effect on the rate of graphene production supports the idea that graphite-to-graphite flake collisions cause the bulk flakes to break apart into smaller pieces, which, in turn, contain layers, held together by weak van der Waals interactions. Smaller fragmented pieces are more easily sheared apart, and so, ultimately increasing graphite-to-graphite collisions enables a higher exfoliation per shear rate.[37,51]

As reported previously, the $[BSA]_i$ shows no effect on the rate of graphene production after a minimum value of 40 μM (Figure 2D). However, the role of BSA in graphene production remains significant. After graphite sheet collisions occur, the BSA molecules immediately catch the ejected graphene fragments on either side and prevent the restacking of multiple graphite sheets together allowing for the high and prolonged stability of graphene flakes in water (Figure 3B). Previous reports suggest that surfactant diffusion and subsequent intercalation between graphene sheets can be an intermediate step to exfoliation by adsorbing to the bottom of one layer and the top of the adjacent layer and causing steric repulsion. With enough BSA adsorption on opposing sides of two adjacent graphene sheets, the layers can push and peel apart from one another.[52] The hydrophobic functional groups on BSA bind to the graphene sheets, while the hydrophilic groups face the solvent (water), thereby allowing for a more favorable interaction and decreasing the graphene's

https://dx.doi.org/10.1021/acsami.9b15121
ACS Appl. Mater. Interfaces 2020, 12, 3815−3826

overall hydrophobicity.[53] The binding of BSA to the graphite and/or graphene surfaces lowers the overall surface free energy.[37] This BSA binding biofunctionalizes the graphene, making it suitable for biological applications.[38,40]

Increasing the sample volume causes a considerable decrease in the graphene rate of production (Figure 2E), most likely due to the decreased shear rate produced. As the solution volume decreased, the percentage of the graphene solution in the reactor experiencing the maximum shear rate caused by the stir bar increases. In turn, this allows for a higher number of graphite-to-graphite collisions throughout and therefore an increase in product formation.

In Figure 2F, the pH of the biographene solution shows little effect on the rate of graphene production as long as the pH is not close to the isoelectric point of BSA (pI = 4.8; range reported in the literature, 4.8−5.2).[54,55] This sheds light on the importance of the charge of BSA in maintaining colloidal stability, which is discussed further in Section 3.3.

To elicit a more cohesive understanding of the underlying mechanism of graphene production via shear force, the reaction order with respect to each of the exfoliation parameters was studied (Figure 1 and Figure S7). The rate equation found for graphene production is given below (eq 2).

$$\text{Rate (mg mL}^{-1}\text{ day}^{-1}) \propto [\text{graphite mg mL}^{-1}]_i^{1.45}\,[\text{BSA }\mu\text{M}]_i^{0}\,(\text{speed, RPM})^{0.31}\,(\text{pH})^{0.06}\,(\text{volume})^{0.74}\,(\text{shear rate})^{1.02} \quad (2)$$

Equation 2 suggests that the initial graphite concentration has the largest effect on biographene production with a reaction order of about 1.5. This heavy influence may be due to the increase in graphite-to-graphite collisions that occur with an increase in graphite concentration, resulting in more fragmented graphite pieces, which are more likely to succumb to shear force and peel apart. It can also be seen in eq 2 that shear rate has the second greatest effect on the biographene production rate due to an increase in shear resulting in an increase in graphene layers being pushed and peeled apart. Further details on the influence of shear rate in the biographene production mechanism are discussed in Section 3.6. Both the speed of the stir bar and the volume of the solution influence the shear rate being applied to the solution so it is intuitive that they both impact the biographene production positively. Equation 2 gives reaction rate orders of 0 and 0.06 for initial BSA concentration and pH, respectively. As can be seen in Figure 2D,F, both the BSA and pH demonstrate no effect on biographene production above a minimum BSA concentration of 40 μM and as long as the pH of the solution is not close to the pI of BSA. For this reason, both of these parameters yield orders of reaction close to or equal to 0 when it comes to the rate of biographene production.

3.3. Characterization of Biographene. Oxidative defects and number of layers of biographene being produced were estimated using Raman spectroscopy. A 514 nm laser was used to excite the biographene samples dried on a glass slide, and the resulting spectrum of biographene is plotted in Figure 3. Biographene exhibits the characteristic graphene Raman peaks at 1348 (D), 1580 (G), 1623 (D′), 2450 (D + D″), 2698 (2D), and 2948 (D + D′) cm^{-1}.[56] In Figure 3B, a clear shift in the 2D band from 2726 to 2698 cm^{-1} and an increase in its intensity from the graphite sample can be seen indicating the change from graphite to a <5 layer sample of graphene.[25,57] It is also important to note the transformation of the 2D band from asymmetric to symmetric in comparing graphite to graphene (FWHM ≈ 80 cm^{-1}).[37,56,57]

From graphite to the biographene sample, there is an increase in the intensity of the D band indicating the presence of edge carbon atoms and disorders, such as corrugations (ripples or wrinkles on the graphene surface) and topological defects such as grain boundaries.[58] Additionally, only the biographene sample exhibits the D′ band, a shoulder peak off of the G peak actuated by graphene sample defects.[56,57] The weak D + D″ band at 2450 cm^{-1} is known and indicated in the literature as a combination mode in samples with defects.[56] The D + D″ band is often cited as the combination mode of the D and D′ peaks.[59] However, we have noted that this peak only seems to appear in samples made with BSA so it is possible that this peak is due to a known BSA C−H stretching mode.[60]

The ratio of the intensity of the D band to the intensity of the D′ band ($I_D/I_{D'}$) was used to determine the level of oxidative defects present in the graphene samples. The $I_D/I_{D'}$ for biographene was calculated to be 2.48, indicating a lack of sp^3 defects and that no oxidative defects were incurred during the exfoliation or during the washing process. It is worth noting that our graphite powder exhibits a weak D band (I_D = 0.02), suggesting that some defects may be due to the starting material (Figure S8). Previous reports suggest that an $I_D/I_{D'}$ ratio below 3.5 implies the presence of edge defects on the sheets.[25,37,59] These edge defects provide further evidence of successful exfoliation of the graphite flakes into graphene and afford easy attachment sites for someone wishing to do conjugation chemistry.

Using the equations (eqs S5−S7) put forth by Paton et al.,[25] it was estimated from the Raman spectra that biographene has an average of three to six layers. An average sheet length of 0.73 ± 0.24 μm was estimated for biographene (Table 1).

Table 1. Average Number of Layers per Biographene Sheet and Average Sheet Length

sample[a]	average number of layers	average sheet length (μm)	sheet $I_D/I_{D'}$
graphite	19.5	149	0.7 ± 0.2
present study, stirred	3−6	0.7 ± 0.2	2.5 ± 0.3
biographene, shear reactor	5−7	1.0 ± 0.1	2.1 ± 0.2
biographene, blender	3−5	0.5 ± 0.1	3.2 ± 0.6

[a]All values were calculated using Raman data and equations put forth by Paton et al. (described in Section S5).[25]

Transmission electron microscopy was used to confirm the formation of sheets via simple stirring and determine the sheet size and shape (Figure 4 and Figure S9). The TEM images show few-layered transparent sheets of biographene, with some curling and stacking of sheets being visible. The average sheet length from TEM was calculated to be 0.61 ± 0.30 μm, matching well with the lateral sizes calculated from the Raman spectra (0.73 ± 0.24 μm). Using ImageJ MGV analysis, we have also calculated the percent transparency of over 150 nanosheets visible in our TEM images. The most common percent transparency found for our samples was between 90−95%, with one-third of the sheets having a transparency of 90% or higher. This correlates well with three- to six-layer graphene sheets if each graphene layer is 97.7% transparent.[6]

The zeta potential (ζ) of the biographene suspensions was measured as a function of pH to further determine the colloidal

https://dx.doi.org/10.1021/acsami.9b15121
ACS Appl. Mater. Interfaces 2020, 12, 3815−3826

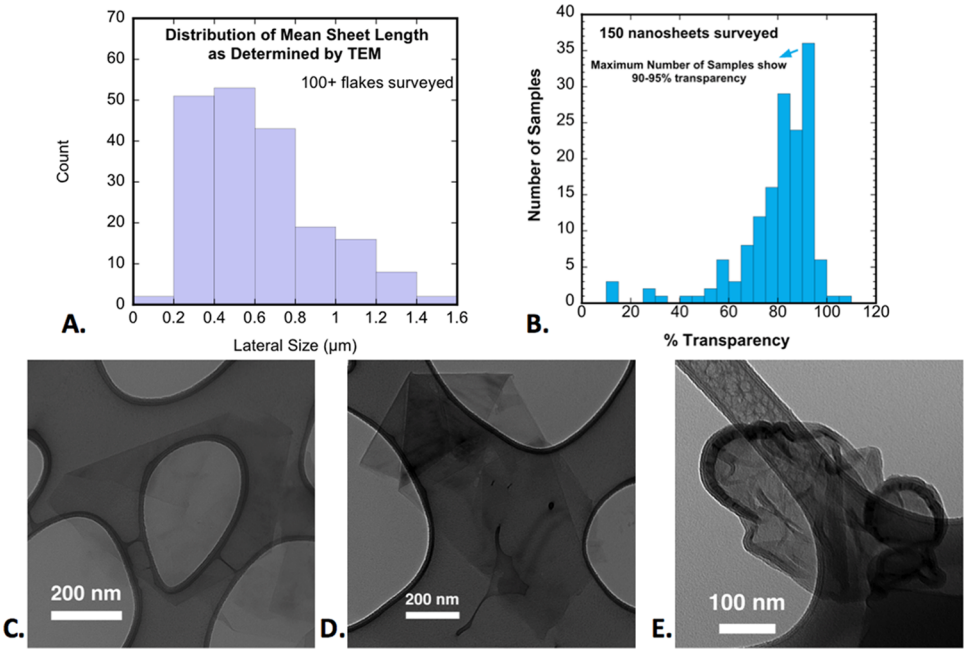

Figure 4. (A) Histogram of biographene flake's lateral size as estimated from TEM images (>100 flakes surveyed). (B) Histogram of the results of an ImageJ analysis of the percent transparency of over 150 sheets surveyed from the TEM data indicating that a majority of the samples have greater than 80% transparency. (C–E) Standard biographene flakes seen using a transmission electron microscope. Transparency of flakes indicates that very few layers are present. Flakes can be seen folding and stacking on one another.

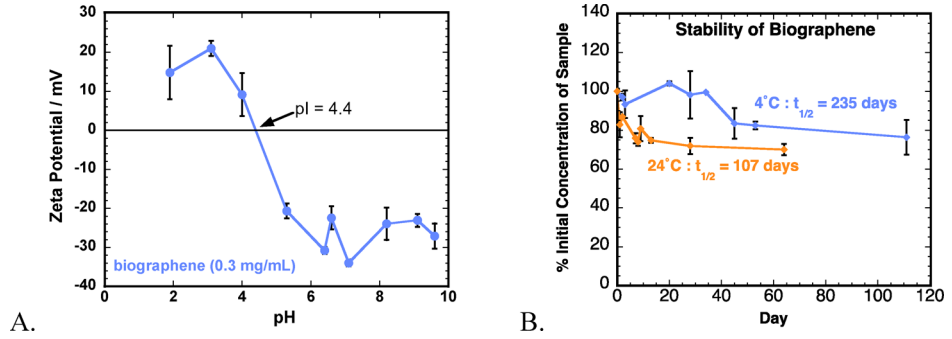

Figure 5. (A) Zeta potential analysis of washed biographene as a function of pH. pH was adjusted with NaOH or HCl before each zeta potential measurement. Ten cycles were run for each of the three trials per pH of the sample. Biographene is seen to be most stable at pH 6–7. (B) Stability of biographene (pH 6.8) at 4 °C (blue) and room temperature, 24 °C (orange). Triplicate samples of each solution were kept in the fridge or on the benchtop, and their UV–vis absorbance at 660 nm was monitored day to day.

stability (Figure 5A). Zeta potential measurements show that the biographene sample is stable over a wide range of pH values, proving to be most stable at pH 7.2. The zeta potential of the solution varied from +15 to −30 mV, as the pH changed from pH 2 to pH 10, indicating that the surface charge on the graphene sheets is heavily influenced by the charge on the protein at that specific pH. These results agree well with the results shown in Figure 2F. In Figure 5A, the isoelectric point was found to be 4.4, which is very close to that of BSA. This allows for the charge on the graphene sheets to be easily tuned by adjusting the pH of the solution.

Both the biographene and unwashed biographene were incredibly stable when kept at 4 °C (refrigerated), showing half-lives of 235 and 262 days, respectively (Figure 5B and Figure S10). Stability was studied by monitoring the sample concentration (UV–vis spectroscopy, 660 nm) from day to day to determine if any of the biographene sheets were degrading and precipitating out of the solution. The stability of the samples was also tested on the benchtop, and the half-life at room temperature for the biographene was estimated to be about 107 days. For research requiring a longer half-life than this, we have found that the addition of 1% benzyl alcohol to the sample solution is able to elongate the half-life, possibly from its bacteriostatic activity.[61] Stability experiments for samples with benzyl alcohol injections were not extensively tested for this study.

3.4. Comparison of the Current Method of Biographene Production with Previous Methods. We have compared our biographene dispersions to graphene dispersions made via other reported methods. The Raman I_D/I_G ratio is often used to determine the level of defects in a graphene sample. In Figure 6A, it can be seen that the I_D/I_G ratio of our graphene sheets is 0.24 ± 0.1, indicating disorders and edge carbons and comparing well with the I_D/I_G of the graphene reported in the literature. However, our sample concentration in water is noticeably higher than those of other synthesis methods. It is important to note that we have chosen to compare to methods using shear force similar to the method presented here.

https://dx.doi.org/10.1021/acsami.9b15121
ACS Appl. Mater. Interfaces 2020, 12, 3815–3826

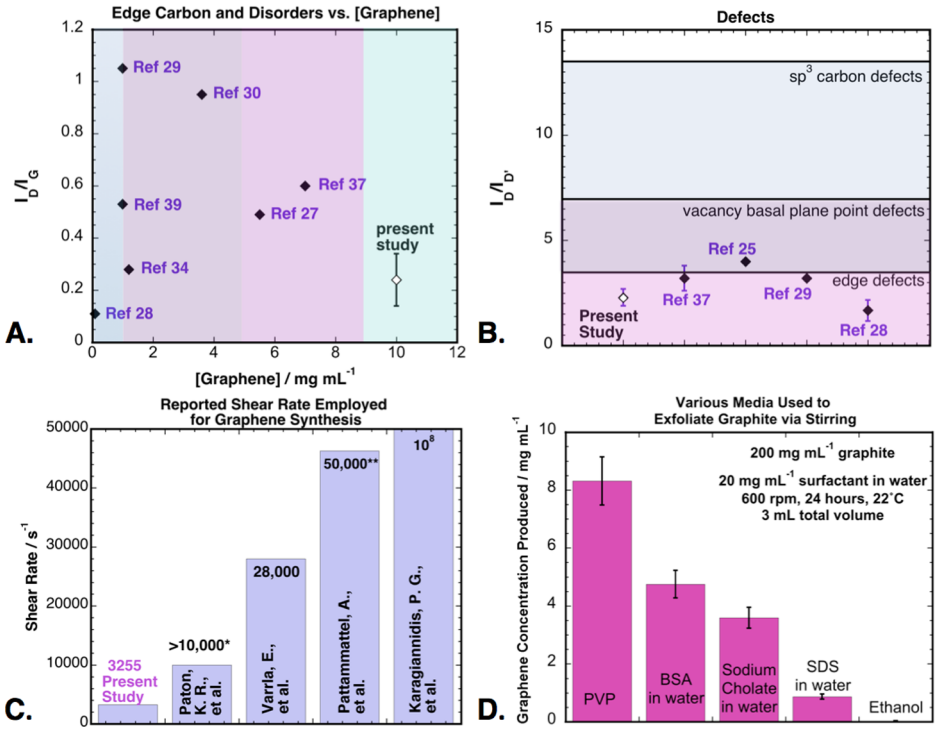

Figure 6. (A) Comparison of reported graphene I_D/I_G values vs. reported graphene concentrations for top-down graphene synthesis methods. (B) Comparison of $I_D/I_{D'}$ values, representative of oxidative defects, reported in the literature for top-down synthesis methods. (C) Comparison of shear rates used for top-down synthesis methods of graphene reported in the literature.[25,32,37,63] (D) Comparison of graphene concentration made after 24 h of stirring graphite in poly(vinylpyrrolidone) (PVP), BSA in water (20 mg mL^{-1}), sodium cholate in water (20 mg mL^{-1}), sodium dodecyl sulfate (SDS) in water (20 mg mL^{-1}), and ethanol.*Reported shear values used were as high as 75,000 s^{-1}.[25] **Shear rate value calculated from reported parameters using equation given by Varrla et al. in eq S4.[32]

However, different methods such as sonication have been known to produce graphene aggregates in water up to 5% by weight.[62] In Figure 6B, the edge defects (inferred from Raman $I_D/I_{D'}$) present in our biographene are shown to compare well with other graphene samples in the literature. Our biographene synthesis method also requires an incredibly small amount of shear force (30−3255 s^{-1}) for graphene synthesis, compared to most methods reported in the literature[25,32,37,63] while also maintaining concentrations up to 10 mg mL^{-1}, as well as low oxidative defects. The comparison of shear rate employed for liquid-phase graphene production in Figure 6C shows that the present method requires a shear rate a factor of about 10 lower than those of other graphene production methods in the literature.

In Figure 6D, we have shown a comparison of graphene concentration made using the present stirring method with different solutions. Graphite (200 mg mL^{-1}) was stirred in poly(vinylpyrrolidone) (PVP), BSA in water (20 mg mL^{-1}), sodium cholate in water (20 mg mL^{-1}), sodium dodecyl sulfate (SDS) in water (20 mg mL^{-1}), and ethanol. The masses of graphene produced after 24 h of stirring in these different media were then compared. The results of this study suggest that both the stir method employed here and the medium in which the graphite is stirred contribute to the overall success of the exfoliation. Graphite stirred in a PVP solution resulted in about 8 mg mL^{-1} graphite in solution, which is higher than most concentrations reported in the literature.[39] Hansen solubility parameters suggest that PVP should solubilize graphene very well in comparison to ethanol.[64] Our results match well with this theory; however, the high concentration of graphene−PVP that was produced suggests that the method of selectively exciting translational modes during the stirring process contributes significantly to the rate of graphene production. The low concentration of graphene produced in ethanol (less than 0.1 mg mL^{-1}) speaks to the idea that the medium used must be able to stabilize/solubilize the exposed graphite surface in order for graphene sheets to be readily pulled off from the graphite crystal. Sodium cholate and SDS are expected to be able to stabilize graphene in water; however, the concentrations produced using this method (3.6 and 0.9 mg mL^{-1}, respectively) appear significantly higher than those reported previously, further justifying the selective activation of the translational modes during shear force liquid-phase exfoliation.[24,39]

We have also compared the concentration of graphene produced using BSA in water (20 mg mL^{-1}) in a shear reactor using the same total rotations used over 24 h in a stir experiment done at 600 rpm (864,000 total rotations). This meant using a shear reactor at 14,400 rpm for a total of 1 h of shear time. This resulted in a biographene concentration of 3.7 ± 0.9 mg mL^{-1}, a slightly lower concentration compared to that of the biographene made via stirring (4.8 ± 0.5 mg mL^{-1}), although they are within error. In comparison, the reported value for graphene concentration made with BSA in water using sonication is about 1 mg mL^{-1}.[44] These comparisons further justify the idea that the method in which graphite is exfoliated into graphene plays just as significant a role as the medium chosen to exfoliate in.

3.5. Test Application of the Biographene. The high electrical and thermal conductivities as well as anticorrosion properties of graphene have made it a desirable coating on aluminum foil for applications such as lithium ion batteries, and light-weight radiators.[65−67] However, coating aluminum with

https://dx.doi.org/10.1021/acsami.9b15121
ACS Appl. Mater. Interfaces 2020, 12, 3815−3826

graphene is often a complicated and extensive process, usually involving chemical vapor deposition or an adhesive layer.[64] The water-soluble graphene sheets reported here were used to easily fabricate stable, flexible FLG coatings on aluminum with no additional adhesive layer by simply drop casting and drying the solution at room temperature. The coatings were stable for months (uncovered) on the benchtop and once dried appear to be unsusceptible to bacterial contamination.

These coatings were thermo-cycled at extreme temperatures (−60 and 80 °C) showing a strong resistance to cracking and peeling (Figures S11 and S12 and eq S8). A single coating of biographene on aluminum was tested with a homemade thermal conductivity device, and the biographene/aluminum sample exhibited superior lateral heat conduction to the uncoated aluminum sample. From these measurements, the thermal conductivity of the graphene in the sample was calculated to be 684 W m^{-1} K^{-1}(Figures S13 and S14 and eq S9). This calculated K value for our graphene (one coat, 2 μm thickness) was about 1.5 times higher than the graphene coating used in the commercial sample (488 W m^{-1} K^{-1}, 40 μm-thick), which required a thermal adhesive to adhere to aluminum (Figure 7 and Table S3). The reported in-plane thermal conductivity of the commercial sample was given as 1600 W m^{-1} K^{-1}; therefore, it may be fair to say that the one-coat biographene sample made in this study would give a K value of about 2400 W m^{-1} K^{-1} if calculated in the same manner; however, this would be quite a stretch and further experimentation is necessary. This is a great step toward easier production of effective graphene/aluminum radiators. As can be seen in Figure 7, our biographene coatings exhibit lateral thermal conductivity values at room temperature that are comparable to those reported in the literature for FLG using a variety of different methods and number of graphene layers.[68−70] Measurements 1−3 in Figure 7 use single multilayer flakes of graphene and are expected to be better than graphene coatings. Measurements 4 and 5 used graphene coatings and were measured using a homemade device (Figure S13).

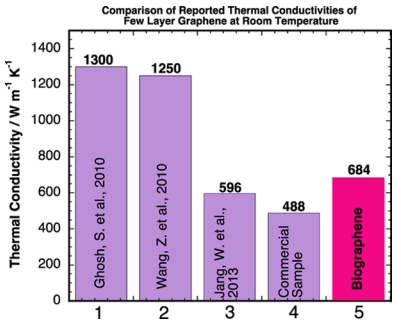

Figure 7. Comparison of FLG lateral thermal conductivity at room temperature reported in the literature. A number of different graphene coatings, as well as methods for measurement, were chosen for comparison ranging from three- to eight-layer graphene, with and without substrates. The lateral thermal conductivity measured for the current study (684 W m^{-1} K^{-1}) compares well with other reports in the literature while also eliminating the need for an adhesive layer on aluminum.[68−70]

The equation developed to calculate lateral thermal conductivity of the samples tested in our apparatus is presented as eq S9. We present these calculations with the understanding that the evaluation of lateral thermal conductivity here is not entirely accurate due to the nature of our homemade device. Interestingly, increasing the number of biographene coatings on aluminum beyond a single coating caused a significant decrease in the calculated thermal conductivity of the graphene (Figure S14). Ghosh et al. report a decrease in thermal conductivity at room temperature in going from a bilayer graphene sample to a four-layer sample of 2800 to 1300 W m^{-1} K^{-1}. They attributed this decrease to cross-plane coupling of low-energy phonons and elegantly explain that despite an increase in heat transport channels with increasing graphene layers, these extra channels do not transmit heat effectively.[68]

Our coating fabrication process is not comparable to that of graphene layers grown via CVD methods as are many of the samples that are tested for thermal conductivity and therefore deserves some discussion here. The through-plane (perpendicular) thermal conductivity value reported for the commercial sample used in this study is 3−5 W m^{-1} K^{-1}. The through-plane thermal conductivity of graphene is said to be restricted by the weak van der Waals interactions that connect graphene layers.[71] It is plausible that the BSA in our graphene sample significantly decreases this perpendicular thermal conductivity value, by further interrupting these van der Waals interactions, thereby causing a higher thermal resistance with increasing sample thickness. Additionally, the room-temperature thermal conductivity of BSA was previously found to be 0.231 W m^{-1} K^{-1} when testing dried BSA films, which is significantly lower than even the through-plane thermal conductivity of graphene.[72] Room-temperature thermal conductivities of graphite and graphite materials range in the literature from 70 to 2200 W m^{-1} K^{-1}.[73]

With increasing biographene coatings on aluminum, there was a noticeable increase in sample surface roughness that may in turn have caused increased contact resistance for thermal conduction between the heat source, sample, and heat sink (Figure S15). This is a possible explanation for why our sample with only one coat of biographene showed significantly higher in-plane thermal conductivity than the samples with more coatings (Figure S14).

The stacking of few-layer biographene inherently deviates from the single-layer graphene that has been shown to have in-plane thermal conductivities as high as 3000−5000 W m^{-1} K^{-1}.[3,66] While coatings of biographene may not be ideal for devices with strict lateral thermal conductivity needs, they could be used effectively in devices requiring heat radiators as well as gradients of heat radiation. Consequently, these coatings on aluminum have a variety of applications in corrosion resistance and lightweight heat radiators.[67]

The decrease in lateral thermal conductivity with increased biographene thickness is not thought to be due to vertical heat transport because the volume of the air surrounding the samples was insulated and because the average temperature of the samples was not much higher than that of the still air immediately surrounding the samples.

In addition to coating our biographene on aluminum and testing the thermal conductivity, we have also coated biographene on cellulose and tested its electrical conductivity (Figure S16) against a known commercial sample. One coating of biographene (0.4 μm) on cellulose paper was found to have a conductivity value of about 1900 S/m, which could potentially be increased with a higher loading.

3.6. Physical Insight Gained from the Current Studies.

The activation energy for a transformation of graphite to graphene was examined by measuring the yield of biographene produced at increasing temperatures at a constant stir speed, and all other conditions were kept constant. A plot of the natural

https://dx.doi.org/10.1021/acsami.9b15121
ACS Appl. Mater. Interfaces 2020, 12, 3815−3826

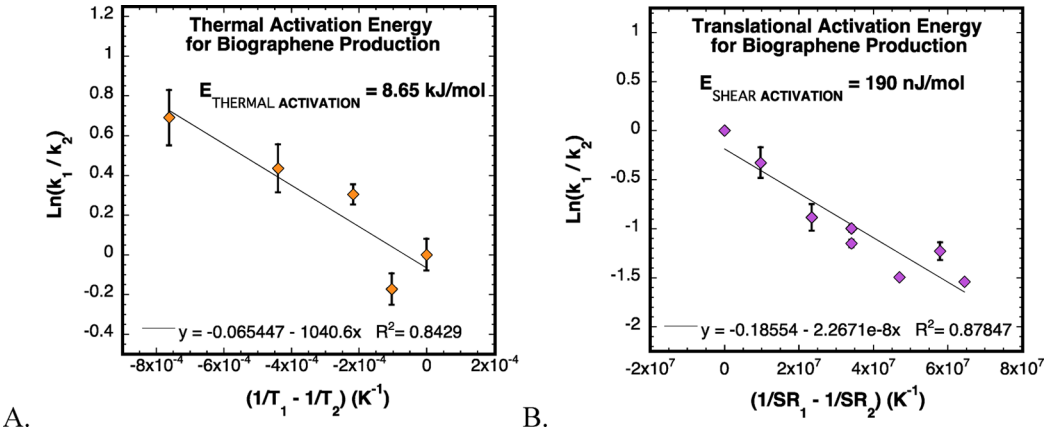

Figure 8. (A) Arrhenius plot used to calculate the thermal activation energy for biographene production in water of 8.65 kJ mol^{-1}. (B) Pseudo-Arrhenius plot constructed to calculate the shear activation energy for biographene production in water of 190 nJ mol^{-1}. In both cases, the slope of the plot was assumed to be equal to $-E_{ACTIVATION}/R$, where R = 8.31 J mol^{-1} K^{-1}.

logarithm of product produced versus $1/T$ resulted in the conventional Arrhenius plot (Figure 8A). The slope of this linear plot gave an activation energy of 8.7 ± 2.2 kJ mol^{-1}. We believe that this is the activation energy required to convert graphite to graphene under normal thermal conditions while stirring. Thermal activation of the system populates all available modes of graphite in compliance with the equipartition theorem. To the best of our knowledge, this key parameter has not been published and provides a useful insight into the activation of the reactant and its conversion to the product, biographene. Since biographene is produced by sliding the graphene from the graphite crystal and subsequent adsorption of BSA onto the separate sheet, we believe that the activation energy corresponds to the sliding of the graphene. We assume that sliding of the graphene sheet is the rate-determining step rather than the binding of the protein to the exposed hydrophobic graphene surface, thereby preventing restacking.

In comparison, we wondered what would be the activation energy for graphene production in a stir reactor where the flowing solvent would transfer some of its energy to the top layers of the graphite crystal, thereby exfoliating graphite. The shear activation energy was measured by quantitating the amount of product produced at increasing shear rates and constant temperatures (20 °C) while keeping all other parameters constant. Surprisingly, a plot of natural logarithm of mass of product produced as a function of 1/(shear rate) yielded a linear plot. Since shear rate has the same units as temperature, this is a pseudo-Arrhenius plot where the temperature is replaced with shear rate. The slope of the plot gave an activation energy of 190 nJ mol^{-1}. The very small value of activation energy for shear-induced exfoliation is surprising but entirely consistent with the idea that exfoliation requires translational motion of the top layer of the crystal. This is further discussed below.

The above two activation energies are astoundingly different, with the former being more than 45 billion times larger than the latter. This affords insight into the energy barriers that must be overcome to exfoliate graphite. Why is the shear activation energy so small? This may be because of the energy distribution into a single translational mode among the $3N$ modes, where N is the number of carbon atoms in a single sheet. When applying shear force, all of the energy transferred from the moving solvent to the surface of the crystal is directed into this single translational mode along the direction of the flow but not the remaining $3N - 1$ modes allowed. Thus, at the most, the shear force populates this single translational mode to produce graphene. Since the solvent flow does not presumably populate rotational or vibrational states, the energy is used extremely efficiently to produce the product, instead of wasting by distribution into the remaining $3N - 1$ modes. For example, thermal activation would populate all $3N$ modes, which include all the translational, rotational, and vibrational modes, thus wasting most of the energy. Therefore, selective translational mode activation is achieved by shear force, making it extraordinarily efficient in exfoliating graphite.

We imagine this to be analogous to a scenario where a ream of paper is placed directly in front of a fan. As the fan blows air at the stack of paper, the sheets will easily go flying off the stack. If, however, the stack of paper was placed on top of a hot plate and heated, it would take a considerably larger amount of heat energy to "remove" a piece of paper from the stack.

In recognizing the differences between these two activation pathways, it can be hypothesized that it is the excited translational states that are giving rise to graphene rather than excited vibrational or other states. The energy barrier measured depends on the modes that are being activated, and therefore, stirring is more energy-efficient by selectively populating the reactive translational state rather than attempting to populate all allowed modes, explaining why such low shear rates can be used to exfoliate graphite. The comparison of these energy barriers offers significant insight into how to structure future graphene exfoliation processes with very high energy efficiencies at room temperature.

4. CONCLUSIONS

In this context, we report a simple method for the synthesis of high-quality, biophilized graphene suspensions in water on an industrial scale. These biographene suspensions are synthesized using only a basic lab stir plate/stir bar to produce a low shear rate and three ingredients: graphite, bovine serum albumin, and water, all of which are environmentally friendly, non-toxic, and inexpensively procured. High concentrations of biographene can be produced continuously and with minimal human intervention using this method. The biographene suspensions produced show no oxidative or sp^3 defects, are three to five layers, and have proven to be stable for over 100 days in solution. The inexpensive biographene coatings of the present study had thermal conductivity values better than commercial samples by

https://dx.doi.org/10.1021/acsami.9b15121
ACS Appl. Mater. Interfaces 2020, 12, 3815−3826

18%, which is highly advantageous for thermal management of spacecrafts. The physical insight gained in the current study implies that translational excitation is an important mechanistic path for graphene production via solvent-mediated exfoliation of graphite. We hypothesize that stir-mediated exfoliation of other layered solids would follow a similar pathway and can be exfoliated efficiently just by stirring. This has not been established, and therefore, the physical insight gained in this study provides new leads in producing other two-dimensional materials in a very energy-efficient manner.

■ ASSOCIATED CONTENT

Supporting Information

The Supporting Information is available free of charge at https://pubs.acs.org/doi/10.1021/acsami.9b15121.

Experimental details for spectroscopy measurements; electron microscopy images; zeta potential analysis; extinction coefficient calculation; Bradford assay; biographene radiator fabrication; thermo-cycling measurements; lateral thermal conductivity measurements; additional results and discussion for BSA removal and quantification; SEM/EDS; TEM; shear rate calculation; activation energy calculation and order of reaction plots; lateral thermal conductivity measurements; and UV−vis characterization of biographene and unwashed biographene (PDF)

Video demonstrating flexibility of biographene coatings on aluminum (MOV)

■ AUTHOR INFORMATION

Corresponding Author

Challa V. Kumar − *University of Connecticut, Storrs, Connecticut;* orcid.org/0000-0002-4396-8738; Email: challa.kumar@uconn.edu

Other Authors

Megan K. Puglia − *University of Connecticut, Storrs, Connecticut;* orcid.org/0000-0001-5470-3500

Sohan Aziz − *University of Connecticut, Storrs, Connecticut*

Kevin M. Brady − *University of Connecticut, Storrs, Connecticut*

Mark O'Neill − *Mark O'Neill, LLC, Fort Worth, Texas*

Complete contact information is available at: https://pubs.acs.org/10.1021/acsami.9b15121

Author Contributions

The manuscript was written through contributions of all authors. All authors have given approval to the final version of the manuscript.

Funding

This work was supported by a NASA STTR subcontract with Mark O'Neill LLC, as well as the University of Connecticut Research Excellence program (OVPR REP).

Notes

The authors declare no competing financial interest.

■ ACKNOWLEDGMENTS

This work was supported by a NASA STTR subcontract with Mark O'Neill LLC, as well as the University of Connecticut Research Excellence program (OVPR REP). The authors thank Dr. Ajith Pattammattel for helpful discussion and Ajitha Chivukula for proofreading the manuscript.

■ REFERENCES

(1) Novoselov, K. S.; Geim, A. K.; Morozov, S. V.; Jiang, D.; Zhang, Y.; Dubonos, S. V.; Grigorieva, I. V.; Firsov, A. A. Electric Field Effect in Atomically Thin Carbon Films. *Science* **2004**, *306*, 666−669.

(2) Novoselov, K. S.; Geim, A. K.; Morozov, S. V.; Jiang, D.; Katsnelson, M. I.; Grigorieva, I. V.; Dubonos, S. V.; Firsov, A. A. Two-dimensional Gas of Massless Dirac Fermions in Graphene. *Nature* **2005**, *438*, 197−200.

(3) Balandin, A. A.; Ghosh, S.; Bao, W.; Calizo, I.; Teweldebrhan, D.; Miao, F.; Lau, C. N. Superior Thermal Conductivity of Single-Layer Graphene. *Nano Lett.* **2008**, *8*, 902−907.

(4) Zhang, Y.; Tan, Y.-W.; Stormer, H. L.; Kim, P. Experimental Observation of the Quantum Hall Effect and Berry's Phase in Graphene. *Nature* **2005**, *438*, 201−204.

(5) Stankovich, S.; Dikin, D. A.; Dommett, G. H. B.; Kohlhaas, K. M.; Zimney, E. J.; Stach, E. A.; Piner, R. D.; Nguyen, S. T.; Ruoff, R. S. Graphene-based Composite Materials. *Nature* **2006**, *442*, 282−286.

(6) Ma, Y.; Zhi, L. Graphene-Based Transparent Conductive Films: Material Systems, Preparation and Applications. *Small Methods* **2019**, *3*, 1800199.

(7) Lee, C.; Wei, X.; Kysar, J. W.; Hone, J. Measurement of the Elastic Properties and Intrinsic Strength of Monolayer Graphene. *Science* **2008**, *321*, 385−388.

(8) Jang, H.; Park, Y. J.; Chen, X.; Das, T.; Kim, M.-S.; Ahn, J.-H. Graphene-Based Flexible and Stretchable Electronics. *Adv. Mater.* **2016**, *28*, 4184−4202.

(9) Kim, K. S.; Zhao, Y.; Jang, H.; Lee, S. Y.; Kim, J. M.; Kim, K. S.; Ahn, J.-H.; Kim, P.; Choi, J.-Y.; Hong, B. H. Large-scale Pattern Growth of Graphene Films for Stretchable Transparent Electrodes. *Nature* **2009**, *457*, 706−710.

(10) Naserpour, M.; Zapata-Rodríguez, C. J.; Vuković, S. M.; Pashaeiadl, H.; Belić, M. R. Tunable Invisibility Cloaking by Using Isolated Graphene-coated Nanowires and Dimers. *Sci. Rep.* **2017**, *7*, 12186.

(11) Edwards, B. C.. The NIAC Space Elevator Program. In *Space 2002 and Robotics 2002*; NASA Institute for Advanced Concepts: 2002.

(12) Han, S.; Wu, D.; Li, S.; Zhang, F.; Feng, X. Porous Graphene Materials for Advanced Electrochemical Energy Storage and Conversion Devices. *Adv. Mater.* **2014**, *26*, 849−864.

(13) Mosa, I. M.; Pattammattel, A.; Kadimisetty, K.; Pande, P.; El-Kady, M. F.; Bishop, G. W.; Novak, M.; Kaner, R. B.; Basu, A. K.; Kumar, C. V.; Rusling, J. F. Ultrathin Graphene-Protein Supercapacitors for Miniaturized Bioelectronics. *Adv. Energy Mater.* **2017**, *7*, 1700358.

(14) Li, X.; Zhu, H.; Wang, K.; Cao, A.; Wei, J.; Li, C.; Jia, Y.; Li, Z.; Li, X.; Wu, D. Graphene-On-Silicon Schottky Junction Solar Cells. *Adv. Mater.* **2010**, *22*, 2743−2748.

(15) Liu, F.; Song, S.; Xue, D.; Zhang, H. Folded Structured Graphene Paper for High Performance Electrode Materials. *Adv. Mater.* **2012**, *24*, 1089−1094.

(16) Li, J.; Niu, L.; Zheng, Z.; Yan, F. Photosensitive Graphene Transistors. *Adv. Mater.* **2014**, *26*, 5239−5273.

(17) Morales-Narváez, E.; Baptista-Pires, L.; Zamora-Gálvez, A.; Merkoçi, A. Graphene-Based Biosensors: Going Simple. *Adv. Mater.* **2017**, *29*, 1604905.

(18) Li, X.; Cai, W.; An, J.; Kim, S.; Nah, J.; Yang, D.; Piner, R.; Velamakanni, A.; Jung, I.; Tutuc, E.; Banerjee, S. K.; Colombo, L.; Ruoff, R. S. Large-Area Synthesis of High-Quality and Uniform Graphene Films on Copper Foils. *Science* **2009**, *324*, 1312−1314.

(19) Yu, Q.; Lian, J.; Siriponglert, S.; Li, H.; Chen, Y. P.; Pei, S.-S. Graphene Segregated on Ni Surfaces and Transferred to Insulators. *Appl. Phys. Lett.* **2008**, *93*, 113103.

(20) Reina, A.; Jia, X.; Ho, J.; Nezich, D.; Son, H.; Bulovic, V.; Dresselhaus, M. S.; Kong, J. Large Area, Few-Layer Graphene Films on Arbitrary Substrates by Chemical Vapor Deposition. *Nano Lett.* **2009**, *9*, 30−35.

(21) Li, X.; Colombo, L.; Ruoff, R. S. Synthesis of Graphene Films on Copper Foils by Chemical Vapor Deposition. *Adv. Mater.* **2016**, *28*, 6247−6252.
(22) Sutter, P. W.; Flege, J.-I.; Sutter, E. A. Epitaxial Graphene on Ruthenium. *Nat. Mater.* **2008**, *7*, 406−411.
(23) Li, X.; Magnuson, C. W.; Venugopal, A.; An, J.; Suk, J. W.; Han, B.; Borysiak, M.; Cai, W.; Velamakanni, A.; Zhu, Y.; Fu, L.; Vogel, E. M.; Voelkl, E.; Colombo, L.; Ruoff, R. S. Graphene Films with Large Domain Size by a Two-Step Chemical Vapor Deposition Process. *Nano Lett.* **2010**, *10*, 4328−4334.
(24) Hernandez, Y.; Nicolosi, V.; Lotya, M.; Blighe, F. M.; Sun, Z.; De, S.; McGovern, I. T.; Holland, B.; Byrne, M.; Gun'Ko, Y. K.; Boland, J. J.; Niraj, P.; Duesberg, G.; Krishnamurthy, S.; Goodhue, R.; Hutchison, J.; Scardaci, V.; Ferrari, A. C.; Coleman, J. N. High-yield Production of Graphene by Liquid-phase Exfoliation of Graphite. *Nat. Nanotechnol.* **2008**, *3*, 563−568.
(25) Paton, K. R.; Varrla, E.; Backes, C.; Smith, R. J.; Khan, U.; O'Neill, A.; Boland, C.; Lotya, M.; Istrate, O. M.; King, P.; Higgins, T.; Barwich, S.; May, P.; Puczkarski, P.; Ahmed, I.; Moebius, M.; Pettersson, H.; Long, E.; Coelho, J.; O'Brien, S. E.; McGuire, E. K.; Sanchez, B. M.; Duesberg, G. S.; McEvoy, N.; Pennycook, T. J.; Downing, C.; Crossley, A.; Nicolosi, V.; Coleman, J. N. Scalable Production of Large Quantities of Defect-free Few-layer Graphene by Shear Exfoliation in Liquids. *Nat. Mater.* **2014**, *13*, 624−630.
(26) Lotya, M.; King, P. J.; Khan, U.; De, S.; Coleman, J. N. High-Concentration, Surfactant-Stabilized Graphene Dispersions. *ACS Nano* **2010**, *4*, 3155−3162.
(27) Unalan, I. U.; Wan, C.; Trabattoni, S.; Piergiovanni, L.; Farris, S. Polysaccharide-assisted Rapid Exfoliation of Graphite Platelets into High Quality Water-dispersible Graphene Sheets. *RSC Adv.* **2015**, *5*, 26482−26490.
(28) Wang, S.; Wang, C.; Ji, X.; Lin, M. Surfactant- and Sonication-free Exfoliation Approach to Aqueous Graphene Dispersion. *Mater. Lett.* **2018**, *217*, 67−70.
(29) Du, W.; Lu, J.; Sun, P.; Zhu, Y.; Jiang, X. Organic Salt-assisted Liquid-phase Exfoliation of Graphite to Produce High-quality Graphene. *Chem. Phys. Lett.* **2013**, *568-569*, 198−201.
(30) Tian, J.; Guo, L.; Yin, X.; Wu, W. The Liquid-phase Preparation of Graphene by Shear Exfoliation with Graphite Oxide as a Dispersant. *Mater. Chem. Phys.* **2019**, *223*, 1−8.
(31) Boothroyd, S. C.; Johnson, D. W.; Weir, M. P.; Reynolds, C. D.; Hart, J. M.; Smith, A. J.; Clarke, N.; Thompson, R. L.; Coleman, K. S. Controlled Structure Evolution of Graphene Networks in Polymer Composites. *Chem. Mater.* **2018**, *30*, 1524−1531.
(32) Varrla, E.; Paton, K. R.; Backes, C.; Harvey, A.; Smith, R. J.; McCauley, J.; Coleman, J. N. Turbulence-assisted Shear Exfoliation of Graphene Using Household Detergent and a Kitchen Blender. *Nanoscale* **2014**, *6*, 11810−11819.
(33) Shinde, D. B.; Brenker, J.; Easton, C. D.; Tabor, R. F.; Neild, A.; Majumder, M. Shear Assisted Electrochemical Exfoliation of Graphite to Graphene. *Langmuir* **2016**, *32*, 3552−3559.
(34) Hou, D.; Liu, Q.; Wang, X.; Qiao, Z.; Wu, Y.; Xu, B.; Ding, S. Urea-assisted Liquid-phase Exfoliation of Natural Graphite into Few-layer Graphene. *Chem. Phys. Lett.* **2018**, *700*, 108−113.
(35) Mandal, P.; Naik, M. J. P.; Saha, M. Room Temperature Synthesis of Graphene Nanosheets. *Cryst. Res. Technol.* **2018**, *53*, 1700250.
(36) Si, Y.; Samulski, E. T. Synthesis of Water Soluble Graphene. *Nano Lett.* **2008**, *8*, 1679−1682.
(37) Pattammattel, A.; Kumar, C. V. Kitchen Chemistry 101: Multigram Production of High Quality Biographene in a Blender with Edible Proteins. *Adv. Funct. Mater.* **2015**, *25*, 7088−7098.
(38) Pattammattel, A.; Pande, P.; Kuttappan, D.; Puglia, M.; Basu, A. K.; Amalaradjou, M. A.; Kumar, C. V. Controlling the Graphene−Bio Interface: Dispersions in Animal Sera for Enhanced Stability and Reduced Toxicity. *Langmuir* **2017**, *33*, 14184−14194.
(39) Guardia, L.; Fernández-Merino, M. J.; Paredes, J. I.; Solís-Fernández, P.; Villar-Rodil, S.; Martínez-Alonso, A.; Tascón, J. M. D. High-throughput Production of Pristine Graphene in an Aqueous Dispersion Assisted by Non-ionic Surfactants. *Carbon* **2011**, *49*, 1653−1662.
(40) Kumar, C. V., Pattammattel, A. *Introduction to Graphene, Chemical and Biochemical Applications*; 1st ed.; Elsevier: August 12 2017; p 232.
(41) Yun-Hwa, P. H., Jack, A. O. *Handbook of Analysis of Edible Animal By-Products*; CRC Press: Boca Raton, Florida, USA, 2011, pp. 13−35.
(42) Bah, C. S. F.; Bekhit, A. E.-D. A.; Carne, A.; McConnell, M. A. Slaughterhouse Blood: An Emerging Source of Bioactive Compounds. *Compr. Rev. Food Sci. Food Saf.* **2013**, *12*, 314−331.
(43) Gu, Z.; Yang, Z.; Wang, L.; Zhou, H.; Jimenez-Cruz, C. A.; Zhou, R. The Role of Basic Residues in the Adsorption of Blood Proteins onto the Graphene Surface. *Sci. Rep.* **2015**, *5*, 10873.
(44) Ahadian, S.; Estili, M.; Surya, V. J.; Ramón-Azcón, J.; Liang, X.; Shiku, H.; Ramalingam, M.; Matsue, T.; Sakka, Y.; Bae, H.; Nakajima, K.; Kawazoe, Y.; Khademhosseini, A. Facile and Green Production of Aqueous Graphene Dispersions for Biomedical Applications. *Nanoscale* **2015**, *7*, 6436−6443.
(45) Alava, T.; Mann, J. A.; Théodore, C.; Benitez, J. J.; Dichtel, W. R.; Parpia, J. M.; Craighead, H. G. Control of the Graphene−Protein Interface Is Required To Preserve Adsorbed Protein Function. *Anal. Chem.* **2013**, *85*, 2754−2759.
(46) Bujacz, A.; Zielinski, K.; Sekula, B. Structural Studies of Bovine, Equine, and Leporine Serum Albumin Complexes with Naproxen. *Proteins: Struct., Funct., Bioinf.* **2014**, *82*, 2199−2208.
(47) Bradford, M. M. A Rapid and Sensitive Method for the Quantitation of Microgram Quantities of Protein Utilizing the Principle of Protein-dye Binding. *Anal. Biochem.* **1976**, *72*, 248−254.
(48) Ladner, T.; Odenwald, S.; Kerls, K.; Zieres, G.; Boillon, A.; Bœuf, J. CFD Supported Investigation of Shear Induced by Bottom-Mounted Magnetic Stirrer in Monoclonal Antibody Formulation. *Pharm. Res.* **2018**, *35*, 215.
(49) Xie, M.-h.; Zhou, G.-z.; Xia, J.-y.; Zou, C.; Yu, P.-q.; Zhang, S.-l. Comparison of Power Number for Paddle-Type Impellers by Three Methods. *J. Chem. Eng. Jpn.* **2011**, *44*, 840−844.
(50) Stark, C. N.; Stark, P. The Relative Thermal Death Rates of Young and Mature Bacterial Cells. *J. Bacteriol.* **1929**, *18*, 333−337.
(51) Yi, M.; Shen, Z. A Review on Mechanical Exfoliation for the Scalable Production of Graphene. *J. Mater. Chem. A* **2015**, *3*, 11700−11715.
(52) Texter, J. A Kinetic Model for Exfoliation Kinetics of Layered Materials. *Angew. Chem., Int. Ed.* **2015**, *54*, 10258−10262.
(53) Shih, C.-J.; Lin, S.; Strano, M. S.; Blankschtein, D. Understanding the Stabilization of Liquid-Phase-Exfoliated Graphene in Polar Solvents: Molecular Dynamics Simulations and Kinetic Theory of Colloid Aggregation. *J. Am. Chem. Soc.* **2010**, *132*, 14638−14648.
(54) Chun, M.-S.; Cho, H. I.; Song, I. K. Electrokinetic Behavior of Membrane Zeta Potential During the Filtration of Colloidal Suspensions. *Desalination* **2002**, *148*, 363−368.
(55) Gaigalas, A. K.; Hubbard, J. B.; McCurley, M.; Woo, S. Diffusion of Bovine Serum Albumin in Aqueous Solutions. *J. Phys. Chem.* **1992**, *96*, 2355−2359.
(56) Ferrari, A. C.; Basko, D. M. Raman Spectroscopy as a Versatile Tool for Studying the Properties of Graphene. *Nat. Nanotechnol.* **2013**, *8*, 235−246.
(57) Ferrari, A. C.; Meyer, J. C.; Scardaci, V.; Casiraghi, C.; Lazzeri, M.; Mauri, F.; Piscanec, S.; Jiang, D.; Novoselov, K. S.; Roth, S.; Geim, A. K. Raman Spectrum of Graphene and Graphene Layers. *Phys. Rev. Lett.* **2006**, *97*, 187401.
(58) Yang, G.; Li, L.; Lee, W. B.; Ng, M. C. Structure of Graphene and its Disorders: A Review. *Sci. Technol. Adv. Mater.* **2018**, *19*, 613−648.
(59) Eckmann, A.; Felten, A.; Mishchenko, A.; Britnell, L.; Krupke, R.; Novoselov, K. S.; Casiraghi, C. Probing the Nature of Defects in Graphene by Raman Spectroscopy. *Nano Lett.* **2012**, *12*, 3925−3930.
(60) Huang, G.; Liu, J.; Jin, W.; Wei, Z.; Ho, C.-T.; Zhao, S.; Zhang, K.; Huang, Q. Formation of Nanocomplexes between Carboxymethyl Inulin and Bovine Serum Albumin via pH-Induced Electrostatic Interaction. *Molecules* **2019**, *24*, 3056.

https://dx.doi.org/10.1021/acsami.9b15121
ACS Appl. Mater. Interfaces 2020, 12, 3815−3826

(61) Lucchini, J. J.; Corre, J.; Cremieux, A. Antibacterial Activity of Phenolic Compounds and Aromatic Alcohols. *Res. Microbiol.* **1990**, *141*, 499−510.
(62) Ager, D.; Arjunan Vasantha, V.; Crombez, R.; Texter, J. Aqueous Graphene Dispersions−Optical Properties and Stimuli-Responsive Phase Transfer. *ACS Nano* **2014**, *8*, 11191−11205.
(63) Karagiannidis, P. G.; Hodge, S. A.; Lombardi, L.; Tomarchio, F.; Decorde, N.; Milana, S.; Goykhman, I.; Su, Y.; Mesite, S. V.; Johnstone, D. N.; Leary, R. K.; Midgley, P. A.; Pugno, N. M.; Torrisi, F.; Ferrari, A. C. Microfluidization of Graphite and Formulation of Graphene-Based Conductive Inks. *ACS Nano* **2017**, *11*, 2742−2755.
(64) Saha, M.; Tambe, P.; Pal, S. Thermodynamic Approach to Enhance the Dispersion of Graphene in Epoxy Matrix and its Effect on Mechanical and Thermal Properties of Epoxy Nanocomposites. *Compos. Interfaces* **2016**, *23*, 255−272.
(65) Wang, M.; Tang, M.; Chen, S.; Ci, H.; Wang, K.; Shi, L.; Lin, L.; Ren, H.; Shan, J.; Gao, P.; Liu, Z.; Peng, H. Graphene-Armored Aluminum Foil with Enhanced Anticorrosion Performance as Current Collectors for Lithium-Ion Battery. *Adv. Mater.* **2017**, *29*, 1703882.
(66) Ghosh, S.; Calizo, I.; Teweldebrhan, D.; Pokatilov, E. P.; Nika, D. L.; Balandin, A. A.; Bao, W.; Miao, F.; Lau, C. N. Extremely High Thermal Conductivity of Graphene: Prospects for Thermal Management Applications in Nanoelectronic Circuits. *Appl. Phys. Lett.* **2008**, *92*, 151911.
(67) Liu, J.; Hua, L.; Li, S.; Yu, M. Graphene Dip Coatings: An Effective Anticorrosion Barrier on Aluminum. *Appl. Surf. Sci.* **2015**, *327*, 241−245.
(68) Ghosh, S.; Bao, W.; Nika, D. L.; Subrina, S.; Pokatilov, E. P.; Lau, C. N.; Balandin, A. A. Dimensional Crossover of Thermal Transport in Few-Layer Graphene. *Nat. Mater.* **2010**, *9*, 555−558.
(69) Wang, Z.; Xie, R.; Bui, C. T.; Liu, D.; Ni, X.; Li, B.; Thong, J. T. L. Thermal Transport in Suspended and Supported Few-Layer Graphene. *Nano Lett.* **2011**, *11*, 113−118.
(70) Jang, W.; Bao, W.; Jing, L.; Lau, C. N.; Dames, C. Thermal Conductivity of Suspended Few-layer Graphene by a Modified T-bridge Method. *Appl. Phys. Lett.* **2013**, *103*, 133102.
(71) Pop, E.; Varshney, V.; Roy, A. K. Thermal properties of graphene: Fundamentals and applications. *MRS Bull.* **2012**, *37*, 1273−1281.
(72) Foley, B. M.; Gorham, C. S.; Duda, J. C.; Cheaito, R.; Szwejkowski, C. J.; Constantin, C.; Kaehr, B.; Hopkins, P. E. Protein Thermal Conductivity Measured in the Solid State Reveals Anharmonic Interactions of Vibrations in a Fractal Structure. *J. Phys. Chem. Lett.* **2014**, *5*, 1077−1082.
(73) Zhou, S.; Chiang, S.; Xu, J.; Du, H.; Li, B.; Xu, C.; Kang, F. Modeling the In-plane Thermal Conductivity of a Graphite/polymer Composite Sheet with a Very High Content of Natural Flake Graphite. *Carbon* **2012**, *50*, 5052−5061.

https://dx.doi.org/10.1021/acsami.9b15121
ACS Appl. Mater. Interfaces 2020, 12, 3815−3826